Neurobiology of Disease

Conditional Forebrain Inactivation of Nicastrin Causes Progressive Memory Impairment and Age-Related Neurodegeneration

Katsuhiko Tabuchi,[1,2]* **Guiquan Chen,**[3]* **Thomas C. Südhof,**[1,2] **and Jie Shen**[3]

[1]Department of Molecular and Cellular Physiology, and Howard Hughes Medical Institute, Stanford University School of Medicine, Palo Alto, California 94304-5543, [2]Department of Neuroscience and Molecular Genetics, and Howard Hughes Medical Institute, University of Texas Southwestern Medical Center, Dallas, Texas 75390, and [3]Center for Neurologic Diseases, Brigham and Women's Hospital, Program in Neuroscience, Harvard Medical School, Boston, Massachusetts 02115

Loss of presenilin function in adult mouse brains causes memory loss and age-related neurodegeneration. Since presenilin possesses γ-secretase-dependent and -independent activities, it remains unknown which activity is required for presenilin-dependent memory formation and neuronal survival. To address this question, we generated postnatal forebrain-specific *nicastrin* conditional knock-out (cKO) mice, in which nicastrin, a subunit of γ-secretase, is inactivated selectively in mature excitatory neurons of the cerebral cortex. *nicastrin* cKO mice display progressive impairment in learning and memory and exhibit age-dependent cortical neuronal loss, accompanied by astrocytosis, microgliosis, and hyperphosphorylation of the microtubule-associated protein Tau. The neurodegeneration observed in *nicastrin* cKO mice likely occurs via apoptosis, as evidenced by increased numbers of apoptotic neurons. These findings demonstrate an essential role of nicastrin in the execution of learning and memory and the maintenance of neuronal survival in the brain and suggest that presenilin functions in memory and neuronal survival via its role as a γ-secretase subunit.

Introduction

Alzheimer's disease (AD) is an age-related neurodegenerative disorder characterized by progressive memory decline, neuronal loss, and formation of amyloid plaques and neurofibrillary tangles (Price et al., 1998). Dominantly inherited mutations in *presenilin* (*PS*) genes, *PS1* and *PS2*, are the primary cause of familial AD (Hardy and Selkoe, 2002). PS forms the γ-secretase complex together with three other subunits: nicastrin, presenilin enhancer 2 (Pen-2), and anterior pharynx defective 1 (Aph-1) (Fortini, 2002). Although the amyloid precursor protein (APP) and Notch receptors are the physiological substrates of γ-secretase, additional substrates have been reported, making it difficult to discern which substrate(s) are the key mediator(s) of PS functions (Brown et al., 2000; Fortini, 2002). Furthermore, evidence has also indicated that PS displays γ-secretase-independent activities, including regulation of β-catenin signaling and control of calcium release from the endoplasmic reticulum (Kang et al., 1999, 2002; LaFerla, 2002; Tu et al., 2006).

Our previous studies demonstrated that conditional inactivation of PSs in the mouse postnatal forebrain results in synaptic dysfunction and impaired learning and memory, followed by age-dependent neuronal loss (Beglopoulos et al., 2004; Saura et al., 2004). It was, however, unclear whether PS maintains memory formation and promotes neuronal survival via its function as a γ-secretase subunit. This question is particularly topical in view of recent studies suggesting that PS may act as a calcium leak channel in the endoplasmic reticulum in a γ-secretase-independent manner (Tu et al., 2006; Bezprozvanny and Mattson, 2008).

Like presenilin, nicastrin is a subunit of the γ-secretase complex (Yu et al., 2000). Nicastrin is a type-1 transmembrane glycoprotein that binds to γ-secretase substrates such as APP and Notch receptors (Yu et al., 2000; Chen et al., 2001) and is required for the cleavage of γ-secretase substrates (Chung and Struhl, 2001; Edbauer et al., 2002; Hu et al., 2002; López-Schier and St. Johnston, 2002). *Nicastrin* germline knock-out ($-/-$) mice die before embryonic day 10.5 (Li et al., 2003a,b; Nguyen et al., 2006). Fibroblasts derived from *nicastrin*$^{-/-}$ embryos are unable to produce Aβ peptides and fail to release the intracellular domain of APP and Notch1 (Li et al., 2003a). Nicastrin probably functions as a "recruiter" protein for substrates by binding to their N-terminal free stub (Shah et al., 2005). However, the physiological role of γ-secretase, in general, and of nicastrin, in particular, in the adult brain remains unknown.

Here, we generated floxed *nicastrin* mutant mice and crossed them with transgenic mice expressing Cre recombinase under control of the *α-calcium-calmodulin-dependent kinase II* (α-

CaMKII) promoter to obtain postnatal forebrain-specific *nicastrin* conditional knock-out (cKO) mice (Yu et al., 2001). Levels of PS and Pen-2 are significantly reduced, whereas the C-terminal fragments of APP (APP-CTFs) accumulate in the *nicastrin* cKO cerebral cortex. *Nicastrin* cKO mice exhibit progressively impaired learning and memory. Furthermore, *nicastrin* cKO mice display age-related neuronal and synaptic loss, accompanied by progressive gliosis. The progressive neuronal loss is likely attributable to apoptotic cell death, as evidenced by increased numbers of apoptotic cells in *nicastrin* cKO mice.

Materials and Methods

Generation of nicastrin *cKO mice.* A 17 kb mouse genomic clone encompassing exons 1–8 of *nicastrin* gene was isolated from 129/SVJ mouse genomic library and subcloned into *Not*I site of pBluescriptII KS(−) for the targeting vector. The *Mul*I site between exons 2 and 3 was mutated to introduce a *Bst*I site where a *neomycin resistance cassette* (*NEO*), surrounded by *flipase recognition target* (*FRT*) and *loxP* site, was inserted for positive selection. Another *loxP* flanked by *Bam*HI site was inserted into *Sma*I site between exons 3 and 4 to allow conditional removal of exon 3. A *diphtheria toxin cassette* (*DT*) was attached to 3′ end of the construct for negative selection. *Asc*I site was introduced outside of *DT* for linearization of the targeting vector. R1 embryonic stem cells (ES cells) were electroporated with the targeting vector, and cell clones resistant to positive and negative selection were screened by Southern analysis using a 3′ outside probe to detect a size shift by *Bam*HI digestion. Homologously recombined clones were isolated and injected into blastocysts of C57BL/6 mice to generate chimeric mice. Germline transmission was screened by PCR for detecting size shift by *loxP* insertion between exons 3 and 4 using primer 1, AGCTCTTCACCAGGTAAGAAC, and primer 2, CTTCAGG-GAAGGACTGTCCAA. The *neomycin resistance cassette* (*NEO*) was removed by flipase recombination by crossing with *flipase* transgenic mice (f*nicastrin* mice).

The generation of α*CaMKII-Cre* transgenic mice was described previously (Yu et al., 2001). To obtain forebrain-specific *nicastrin* cKO (f*nicastrin*/f*nicastrin;CaM-Cre* or f*nicastrin*/*nicastrin*$^\Delta$*;CaM-Cre*) mice, we crossed floxed *nicastrin* (f*nicastrin*/f*nicastrin*) mice with α*CaMKII-Cre* Tg mice. Homozygous f*nicastrin*/f*nicastrin* mice were generated in C57BL/6129 hybrid background, whereas α*CaMKII-Cre* transgenic mice were generated in C57BL/6CBA hybrid strain and then backcrossed to B6 for >10 generations. Therefore, the genetic background of all the mice used in this study was C57BL/6129 hybrid. *PS* double conditional knockout (*PS* cDKO) mice were reported previously (Saura et al., 2004). The experimenters of molecular, behavioral, and morphological studies were blind to the genotypes of the mice.

Lentivirus production. Lentivirus vectors carrying either nuclear localization signal (NLS)-EGFP or EGFP-NLS-Cre recombinase fusion gene (Ho et al., 2006) were transfected into HEK293T cells together with the HIV-1 packaging vector 8.9, and the VSVG (vesicular stomatitis virus glycoprotein) envelope glycoprotein using FuGENE6 reagent. Transfected cells were cultured for 48 h in MEF media or neuron culture medium. Supernatants were filtrated with 0.48 μm filter unit and stored at −80°C until use.

Generation of nicastrin$^{-/-}$ *cell lines.* Embryonic day 13.5 embryos were removed from uteri and placed into PBS in Petri dishes. Heads, livers, and hearts were removed, and remains were minced into small pieces. They were then transferred into 1.5 ml Eppendorf tubes. A total of 0.2 ml of 1× trypsin/EDTA was added and incubated at 37°C for 10 min. One milliliter of MEF media (DMEM, 20% fetal bovine serum, 2 mM glutamine, 0.1 mM nonessential amino acids, 1 mM sodium pyruvate, 50 μg/ml penicillin/streptomycin, 0.00007% β-mercaptoethanol) was added to inactivate trypsin followed by pipetting to dissociate the cells. Cells were transferred into six-well dishes and cultured in 4 ml of MEF media at 37°C. When cells became confluent [∼2 d in vitro (DIV2)], they were trypsinized and transferred into 10 cm dishes. Small aliquots were kept for genotyping. f*nicastrin*/− cells were immortalized by transfection with pCMV-SV40 large-T antigen using FuGENE6. *Nicastrin* KO cell

lines (−/−) were generated from f*nicastrin*/− cell lines by Cre recombination using Cre-expressing lentivirus.

Neuron cultures. Hippocampi were dissected from newborn floxed *nicastrin* mice and minced into small pieces. They were treated with 5 mg/ml trypsin for 10 min at 37°C after several washes with HBSS. Trypsin was washed out with HBSS plus 20% FBS solution and replaced with plating medium (MEM high-glucose medium containing 10% FBS, transferrin, and insulin). Neurons were dissociated in the plating media by trituration with siliconized Pasteur pipettes and plated on Matrigel-coated coverslips in 24-well plates. They were cultured in similar medium containing B-27 supplement and 4 μM cytosine arabinoside to suppress glial growth at 37°C in a humidified incubator gassed with 95% air and 5% CO_2. One-half volume of medium was replaced with virus-containing media at DIV4. DIV14 cultures were harvested for Western analysis.

Stereology. Brains were perfused with PBS, fixed in 10% formalin, processed for paraffin embedding, and serially sectioned (10 μm). Sagittal brain sections were deparaffinized, alcohol dehydrated, and stained with 0.5% cresyl violet (Nissl) or immunostained with monoclonal antibodies raised against microtubule-associated protein 2 (MAP2) (1:200; Sigma-Aldrich), synaptophysin (1:200; Sigma-Aldrich), glial fibrillary acidic protein (GFAP) (1:500; Sigma-Aldrich), and incubated with either Alexa Fluor 488 goat anti-mouse or Alexa Fluor 594 goat anti-mouse secondary antibodies (Invitrogen), and then analyzed with a Zeiss 510 confocal laser-scanning microscope. Neuron counts were performed using the optical dissector technique (West and Gundersen, 1990) in 10 μm paraffin sagittal sections stained with cresyl violet. Neuronal number and volume of a neocortical hemisphere were determined as described previously (Saura et al., 2004).

Immunoblotting. The mice cortices were dissected and homogenized in cold radioimmunoprecipitation assay lysis buffer [consisting of the following (in mM): 20 mM Tris-HCl, pH 7.4, 150 mM NaCl, 1 mM EDTA, 1% NP-40, 0.5% sodium deoxycholate, and 0.1% SDS] containing protease and phosphatase inhibitors (Sigma-Aldrich). Lysates were cleared by centrifugation (12,000 rpm for 15 min). Normalized volumes of samples were resolved in 4–12% SDS-PAGE, transferred to nitrocellulose membrane, and immunoblotted using infrared dye-coupled secondary antibodies (goat anti-rabbit IRdye800, goat anti-mouse IRdye680, goat anti-rabbit IRdye680, and goat anti-mouse IRdye800 from Li-Cor). Image acquisition and data quantitation were performed using Odyssey Infrared Imaging System (Li-Cor). Primary antibodies used were as follows: anti-nicastrin (N1660; 1:500; Sigma-Aldrich), anti-PS1-CTF (1:1000; Millipore Bioscience Research Reagents), anti-PS1-NTF (1:8000; Millipore Bioscience Research Reagents), anti-Pen-2 (1:200; Zymed), anti-Aph-1a (1:200; Zymed), anti-APP (C8; 1:1000), anti-αAPPs (1:1000), anti-GFAP (1:500; Sigma-Aldrich), anti-Iba1 (1:1000; Wako), anti-VCP (valosin-containing protein) (1:200; Santa Cruz), and anti-β-actin (1:30,000; Abcam).

TUNEL staining. The brain sections were blocked using 5% of goat serum for 30 min followed by the treatment of fluorescein (Roche) at 37°C for an hour. The slides were then washed using TBS for three times. Terminal deoxynucleotidyl transferase-mediated biotinylated UTP nick end labeling (TUNEL) staining was analyzed using a Zeiss 510 confocal laser-scanning microscope.

The Morris water maze. The water maze is a circular pool (160 cm in diameter). During the hidden platform training, the platform (10 cm in diameter) was kept submerged under water and maintained in the same position. Mice were given six trials of training per day (two trials per block; ∼2 h interblock interval) for 7 d, and they were released from all four quadrants in a pseudorandom manner. During the 60 s training period, if the mice were unable to locate the hidden platform, they were guided to the platform by hand and allowed to remain on it for 30 s. The swimming of the mice was monitored using an automated tracking system (HVS Image). After training days 5 and 7, the mice were subjected to a 60 s probe trial in which the platform was removed and the mice were allowed to search for it. Ideally, the mice should be released from all four quadrants in a pseudorandom manner during the probe trial, but we released all mice from the opposite quadrant, since the number of mice we had per genotype was not an exact multiple of 4 (for four quadrants).

In addition, our previous studies using both methods resulted in similar conclusions (Yu et al., 2001; Saura et al., 2004). In the visible platform test, the platform was raised above water and marked by a black-and-white golf ball.

Contextual fear conditioning. For contextual fear conditioning, on training day, mice were placed within the conditioning chamber for 3 min before the onset of the unconditioned stimulus (footshock). After a 1 s/1mA single footshock, they were allowed to remain in the chamber for an additional 2 min and then returned to their home cages. Mice were tested 24 h after training for 4 min in the same conditioning chamber. Mice from all genotype groups responded to the footshock similarly by jumping and vocalization. Freezing was defined as a complete cessation of movement except for respiration and scored by an automated system (Actimetrics).

Open field test. VersaMax system from AccuScan Instruments (Columbus Instruments) was used to study locomotor functions of the mice. Two 42 × 42 cm Plexiglas chambers were set in a quiet laboratory room. The open-field chamber is divided by 16 horizontal infrared beams from left to right, 16 horizontal infrared beams from front to back on the floor. The mice were allowed to get habituated in the experimental room for 30 min before the test started. During the test, the mouse was placed in the center of the open-field chamber and allowed to ambulate in it for 15 min. After each testing trial, the chambers were thoroughly cleaned to remove any odors left by animals tested in a previous trial. Movements of the animals were tracked by the VersaMax system.

Rotarod test. The mice were placed in a neutral position on a stationary 6-cm-diameter accelerating rotarod (Economex; Columbus Instruments), which is equipped with individual timers and allows four mice to be tested at a time. Mice were first trained to stay on the rod at a constant rotation speed of 5 rpm. Mice unable to stay on the rod for 2 min were placed back on the rod until they did not fall from the rod for 2 min (pretraining). After successful pretraining, mice were placed back on the rod at a rotation speed of 5 rpm. The rotating speed is then increased at a rate of 0.2 rpm/s. The latency to fall was measured. All mice were tested for three trials in total on the same experimental day.

Data analysis. Statistical analyses were performed using ANOVA to measure genotype, age effect or genotype by age interaction effect. Two-tailed Student's t test was conducted for all the pairwise comparisons in the behavioral and biochemical results. Unless otherwise stated, three to six mice were used per genotype group. A value of $p < 0.05$ is considered significant. All the data were reported as mean ± SEM throughout.

Results

Generation of postnatal forebrain-restricted *nicastrin* cKO mice

To inactivate nicastrin selectively in the postnatal forebrain, we first generated floxed *nicastrin* mice, in which exon 3 is flanked by two *loxP* sites (Fig. 1*A*). We introduced a *loxP* sequence into intron 3 and another *loxP* site together with a selection cassette,
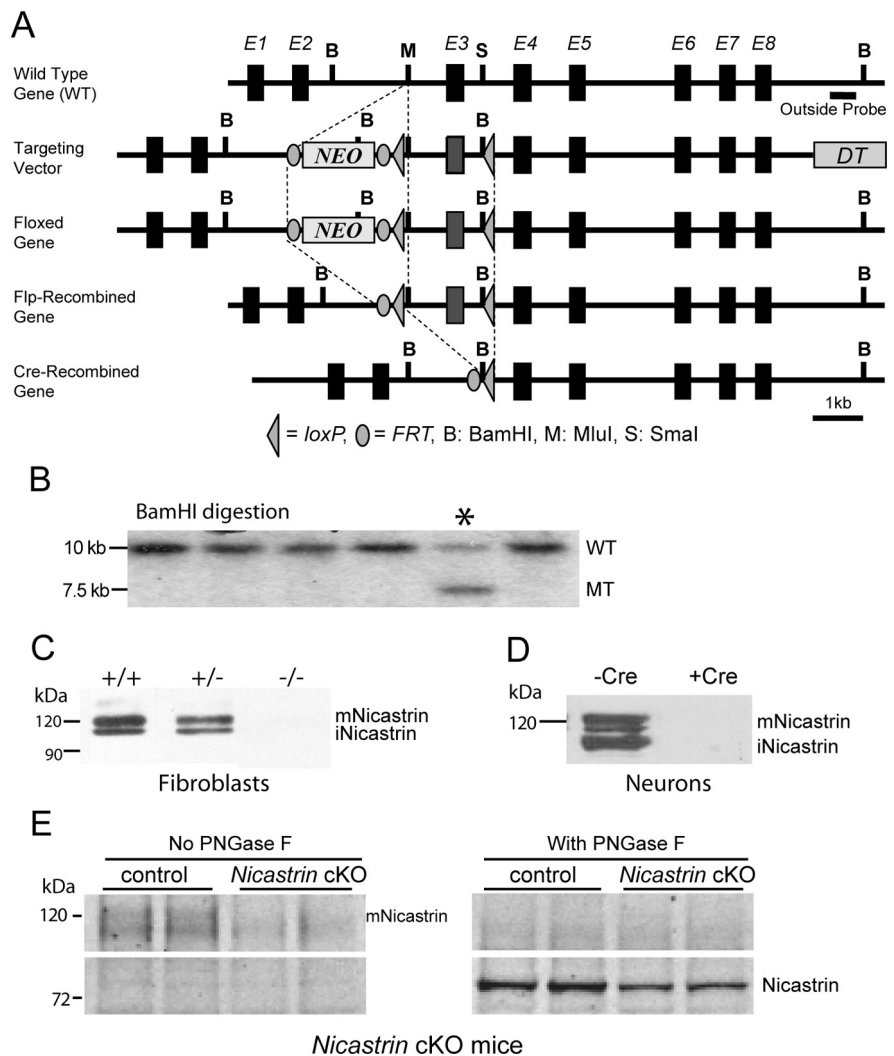
Figure 1. Generation of *nicastrin* cKO mice. ***A***, Targeting strategy. Exon 3 of the *nicastrin* gene was flanked by two *loxP* sites (gray arrowheads) and a *NEO* selection cassette with two *FRT* sites (gray circles). The diagram is not drawn to scale. ***B***, Southern blot screening for properly recombined ES cells. Genomic DNA extracted from transfected ES cells was digested with *Bam*HI and blotted with a 3′ outside probe. The presence of the 7.5 kb *Bam*HI fragment indicates the occurrence of the proper homologous recombination event in ES cells, which represents the mutant allele and is indicated by the asterisk. WT, Wild-type band; MT, mutant band. ***C***, Fibroblasts derived from f*nicastrin*/− mice were immortalized by SV40 large-T antigen transfection and infected with lentivirus expressing Cre recombinase to establish *nicastrin* KO cell line (−/−). No mature or immature nicastrin protein is detected in *nicastrin* KO fibroblasts. "mNicastrin" denotes mature nicastrin. "iNicastrin" denotes immature nicastrin. ***D***, Neuronal cultures prepared from newborn f*nicastrin*/f*nicastrin* mice were infected with either the control (-Cre) or Cre lentiviruses at DIV4. Lysates were collected at DIV14 and immunoblotted for nicastrin. Neither mature nor immature nicastrin protein is detected in *nicastrin* KO cultured neurons, indicating that introduction of Cre eliminates nicastrin expression. ***E***, Immunoblotting of nicastrin in forebrain-specific *nicastrin* cKO mice at 2 months of age. Cortical lysates were nontreated or treated with PNGase-F to deglycosylate nicastrin. Levels of deglycosylated nicastrin protein are reduced at ∼50% in the *nicastrin* cKO cortex. The asterisk denotes statistical significance (*$p < 0.05$).

which encodes *neomycine resistance* (*NEO*) and is flanked by two *FRT* (*flipase recognition target*) sites, into intron 2 (Fig. 1*A*). The targeting vector was transfected into R1 embryonic stem (ES) cells, and the resulting ES cell clones were screened by Southern analysis using a 3′ external probe (Fig. 1*B*). Positive ES cell clones carrying the proper homologous recombination event were further confirmed by PCR, and then injected into mouse blastocysts to generate chimeric mice, which were bred with C57BL/6J mice. To remove the *NEO* selection cassette, we crossed F_1 heterozygous mice with *flp* deleter mice (Dymecki, 1996) and generated floxed *nicastrin* mice. We also crossed floxed *nicastrin* mice to *protamine-Cre* transgenic (Tg) mice, in which Cre recombinase is
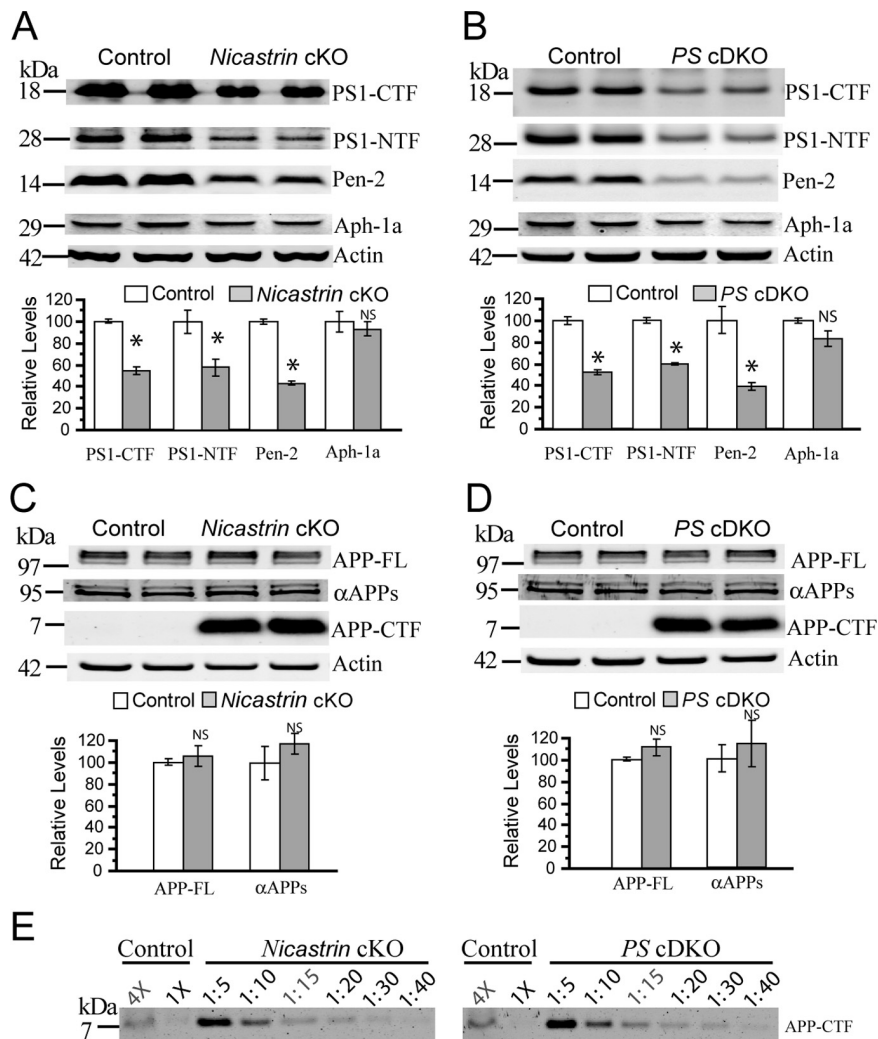
Figure 2. Levels of γ-secretase subunits and APP cleaved products in *nicastrin* cKO and *PS* cDKO mice at 2 months of age. **A**, Significant reductions of the levels of PS1-CTF, PS1-NTF, and Pen-2 but unchanged levels of Aph-1a in *nicastrin* cKO mice. Cortical lysates from *nicastrin* cKO and control mice were analyzed by immunoblotting (top) using antibodies against PS1-CTF, PS1-NTF, Pen-2, and Aph-1a. Protein levels were standardized with β-actin (bottom). The asterisk denotes statistical significance (*$p <$ 0.05). NS denotes not significant. **B**, Reductions of γ-secretase subunits in *PS* cDKO mice. Conditional removal of *PSs* results in a ~50% reduction of PS1-CTF and PS1-NTF levels, which is similar to the observation in *nicastrin* cKO. Reduced levels of Pen-2 but unchanged levels of Aph-1a are observed in *PS* cDKO mice. Cortical lysates from *PS* cDKO and control mice were analyzed by immunoblotting (top). Protein levels were standardized with β-actin (bottom). The asterisk denotes statistical significance (*$p < 0.05$). **C, D**, Unchanged levels of APP full-length (APP-FL) and soluble APP-α fragment (αAPPs) in *nicastrin* cKO (**C**) and *PS* cDKO mice (**D**). Immunoblotting (top) was conducted using antibodies specific for APP-FL and αAPPs. Protein levels were standardized with β-actin (bottom). Quantification analysis shows no significant changes in protein levels for APP-FL and αAPPs but a massive increase in protein levels for APP-CTFs in *nicastrin* cKO and *PS* cDKO mice, relative to those in control mice. **E**, Direct comparison of immunoblotting on APP-CTFs in *nicastrin* cKO and *PS* cDKO mice at 2 months of age. Cortical lysates prepared from *nicastrin* cKO and *PS* cDKO mice were diluted as indicated (lanes 3–8) and immunoblotted with the APP C8 antibody. Undiluted homogenate (1×) and four times of the undiluted homogenate (4×) from control mice were also immunoblotted. The levels of APP-CTFs in *nicastrin* cKO and *PS* cDKO cortex were increased ~60-fold relative to those of the control mice.

expressed in male germ cells, to generate germline *nicastrin* KO (*nicastrin*$^{-/-}$) mice.

Since *nicastrin*$^{-/-}$ mice exhibited early embryonic lethality, we examined levels of nicastrin protein in *nicastrin*$^{-/-}$ fibroblasts. Fibroblasts derived from embryos carrying *nicastrin* floxed and deleted alleles (f*nicastrin*/−) at day 13.5 were immortalized and infected with the lentivirus expressing Cre recombinase to establish *nicastrin*$^{-/-}$ cells. No nicastrin protein was detected in *nicastrin*$^{-/-}$ cells (Fig. 1C), whereas ~50% nicastrin protein was observed in *nicastrin*$^{+/-}$ cells, compared with wild-type cells. Moreover, when we infected cultured primary cortical neurons

derived from newborn f*nicastrin*/f*nicastrin* mice with a lentivirus expressing Cre recombinase, nicastrin levels were undetectable in these neurons (Fig. 1D), confirming that the presence of Cre eliminates nicastrin expression.

Postnatal forebrain-specific *nicastrin* cKO mice were generated by crossing f*nicastrin*/f*nicastrin* mice to transgenic mice that express Cre recombinase specifically in excitatory neurons of postnatal forebrain under the control of the αCaMKII promoter (Yu et al., 2001). To determine the level of nicastrin in the cortex of *nicastrin* cKO mice, we prepared cortical lysates at 2 months of age and performed Western analysis (Fig. 1E). Since nicastrin is modified by posttranslational glycosylation, we also treated the cortical lysates with peptide-*N*-glycosidase F (PNGase F) to remove saccharide groups from the mature glycosylated form of nicastrin proteins, and then performed Western analysis. We found a reduction of ~50% in the levels of the deglycosylated form of nicastrin in *nicastrin* cKO mice at this age (Fig. 1E). The residual amount of nicastrin in these mice may be attributable to the expression of nicastrin in glia, interneurons, and a small percentage of excitatory neurons that lack Cre expression.

Reduced levels of γ-secretase components and impaired APP processing in *nicastrin* cKO mice

To determine the effects of nicastrin inactivation on other components of the γ-secretase complex, we measured the levels of PS1, Pen-2, and Aph-1a in cortical lysates of 2-month-old *nicastrin* cKO mice. We found a 50% of reduction in the C-terminal (PS1-CTF) and N-terminal fragments of PS1 (PS1-NTF), suggesting that inactivation of nicastrin significantly affects protein levels of PS1 (Fig. 2A). We observed a ~60% reduction in Pen-2 levels (Fig. 2A). In contrast, levels of Aph-1a were unchanged in *nicastrin* cKO mice (Fig. 2A). These results suggest that inactivation of nicastrin significantly affects protein levels of other components of the γ-secretase complex, consistent with previous findings (Steiner et al., 2002; Gu et al., 2003). In parallel, we also measured the levels of PS1-CTF, PS1-NTF, Pen-2, and Aph-1a in cortical lysates of 2-month-old *PS* cDKO mice. We found comparable reductions on PS1-CTF, PS1-NTF, and Pen-2 levels, but no significant change on Aph-1a levels (Fig. 2B).

Next, we examined whether loss of nicastrin alters APP processing in the adult cerebral cortex. Western analysis revealed normal levels of APP full-length (APP-FL) protein in *nicastrin* cKO mice (Fig. 2C), indicating that nicastrin inactivation does not alter the expression of APP. Levels of soluble APPα (αAPPs) were also normal in the cortex of *nicastrin* cKO mice (Fig. 2C).

APP C-terminal fragments (APP-CTFs), however, accumulated in the cortex of *nicastrin* cKO mice (Fig. 2*C*). Similarly, Western analysis of cortical lysates of *PS* cDKO mice at 2 months indicated that levels of APP-FL and αAPPs were not changed (Fig. 2*D*), but levels of APP-CTFs were significantly increased (Fig. 2*D*).

To quantify the extent of increases in APP-CTFs, we performed Western analysis using a serial dilution of *nicastrin* cKO cortical lysates at 2 months of age (Fig. 2*E*). We found that APP-CTFs levels in *nicastrin* cKO mice were increased ~60-fold, relative to those in the control. Furthermore, we similarly compared levels of APP-CTFs in *nicastrin* cKO mice with those in *PS* cDKO mice at the same age and found that levels of APP-CTFs were also increased ~60-fold in *PS* cDKO mice (Fig. 2*E*). These results indicate that, like PS, nicastrin is essential for γ-secretase-mediated processing of APP.

Normal brain morphology in *nicastrin* cKO mice at 2 months

Although *nicastrin*$^{-/-}$ mice exhibit embryonic lethality (Li et al., 2003a,b), *nicastrin* cKO mice were viable and visually indistinguishable from their littermate controls during early adulthood. To address whether inactivation of nicastrin affects brain morphology, we performed Nissl staining using brain sections from *nicastrin* cKO mice at 2 months of age. Nissl-stained histology revealed grossly normal brain architecture in cKO mice (Fig. 3*A*). Unbiased stereological counting of neurons in the cKO cortex uncovered no significant changes in total cortical neuronal number ($F = 1.3$; df = 1, 4; $p > 0.3$), or in cortical ($F < 1$) and hippocampal volumes ($F < 1$) (data not shown). Immunohistological analysis revealed no significant changes in immunoreactivities of MAP2 and synaptophysin (SVP38) in the neocortex and the hippocampus, suggesting normal dendrites and synapses in *nicastrin* cKO mice (Fig. 3*B,C*). These results indicate no detectable changes in brain morphology and total cortical neuronal number in *nicastrin* cKO mice at 2 months.

Progressive impairment of spatial learning and memory in *nicastrin* cKO mice

To test whether loss of nicastrin affects learning and memory, we examined hippocampus-dependent spatial learning in *nicastrin* cKO and littermate control mice at 2–3 and at 7–8 months of age, using the Morris water maze (MWM) task (Morris et al., 1982). We trained the mice to learn the location of a hidden platform in the MWM for 7 d [for acquisition curves, see Fig. 4*A* (2–3 months), *B* (7–8 months)]. First, we performed an ANOVA to evaluate overall effects for all mice. The ANOVA revealed a highly significant within-subject effect during training ($F = 42.9$; df = 4.6, 210.7; $p < 0.0000001$) as expected. The overall ANOVA also revealed a highly significant main genotype effect ($F = 27.9$; df = 1, 46; $p < 0.00001$), suggesting impaired spatial learning in *nicastrin* cKO mice. We further compared the behavioral performance for each age separately, and confirmed a significant genotype effect (2–3 months; $F = 5.4$; df = 1, 22; $p < 0.05$; 7–8 months;
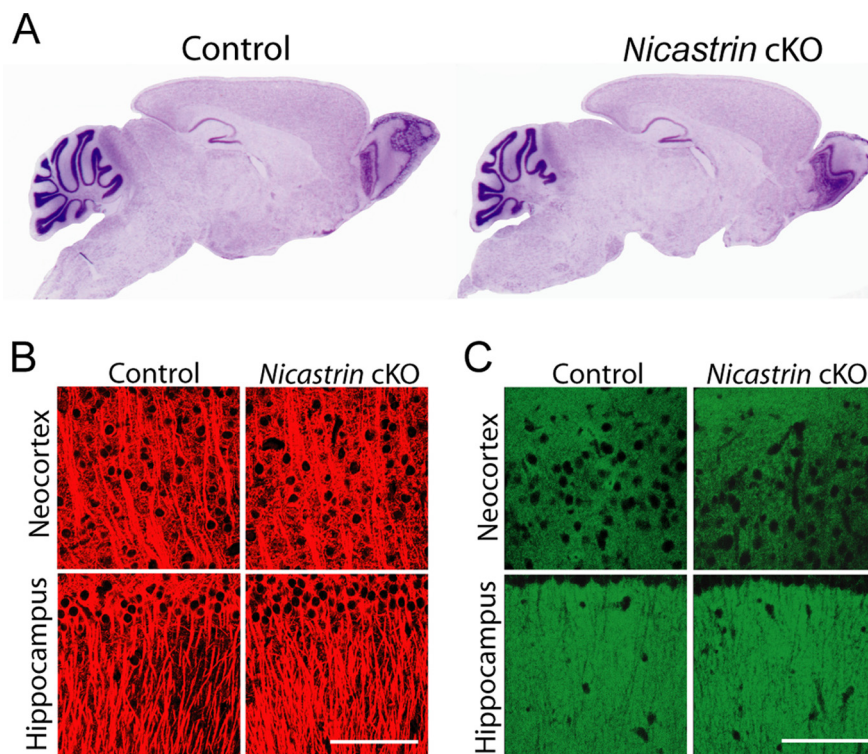
Figure 3. Normal brain morphology of *nicastrin* cKO mice at 2 months. ***A***, Normal brain cytoarchitecture, including the neocortex and hippocampus, revealed by Nissl staining of sagittal sections from *nicastrin* cKO and control brains. ***B***, Comparable MAP2 immunoreactivity in the neocortex and hippocampal area CA1 of cKO and control brains. ***C***, Comparable synaptophysin (SVP38) immunoreactivity in the neocortex and hippocampal area CA1 of cKO and control brains. Scale bar, 100 μm.

$F = 32.0$; df = 1, 24; $p < 0.00001$). Furthermore, the overall ANOVA showed a highly significant age effect in *nicastrin* mutant mice ($F = 28.2$; df = 1, 23; $p < 0.00001$) but only a "trend" in control mice ($F = 3.54$; df = 1, 23; $p = 0.07$). Overall, these results indicate that *nicastrin* cKO mice exhibit a progressive impairment in spatial learning.

After the MWM training, the mice were subjected to a probe test, in which the hidden platform was removed from the water maze and the mice were allowed to swim freely in search for the former platform location in the target quadrant (Fig. 4*C*, 2–3 months; *D*, 7–8 months). First, we conducted an overall ANOVA to compare the time spent in the target quadrant and the other three quadrants by all mice. We found a significant quadrant effect ($F = 6.0$; df = 1, 30; $p < 0.025$), suggesting a searching preference to the target quadrant after the training. Second, we performed an overall ANOVA to compare the time spent in the target quadrant, and found a significant genotype effect ($F = 10.9$; df = 1, 30; $p < 0.005$), consistent with impaired spatial memory in *nicastrin* cKO mice. We then conducted data analysis for 2–3 and 7–8 months separately. We found a significant genotype effect on the time spent in the target quadrant for 2–3 months ($F = 8.8$; df = 1, 22; $p < 0.01$) (Fig. 4*C*) and a highly significant genotype effect for 7–8 months ($F = 13.2$; df = 1, 24; $p < 0.001$) (Fig. 4*D*). Figure 4, *E* and *F*, show swim paths during the probe trial for 2–3 and 7–8 months groups, respectively. Both younger and older control mice spent much more time in the target quadrant than the age-matched *nicastrin* cKO mice, providing additional evidence for a progressive impairment in spatial memory in *nicastrin* cKO mice.

To exclude the possibility that the impairment in spatial memory in young *nicastrin* cKO mice is secondary to abnormal
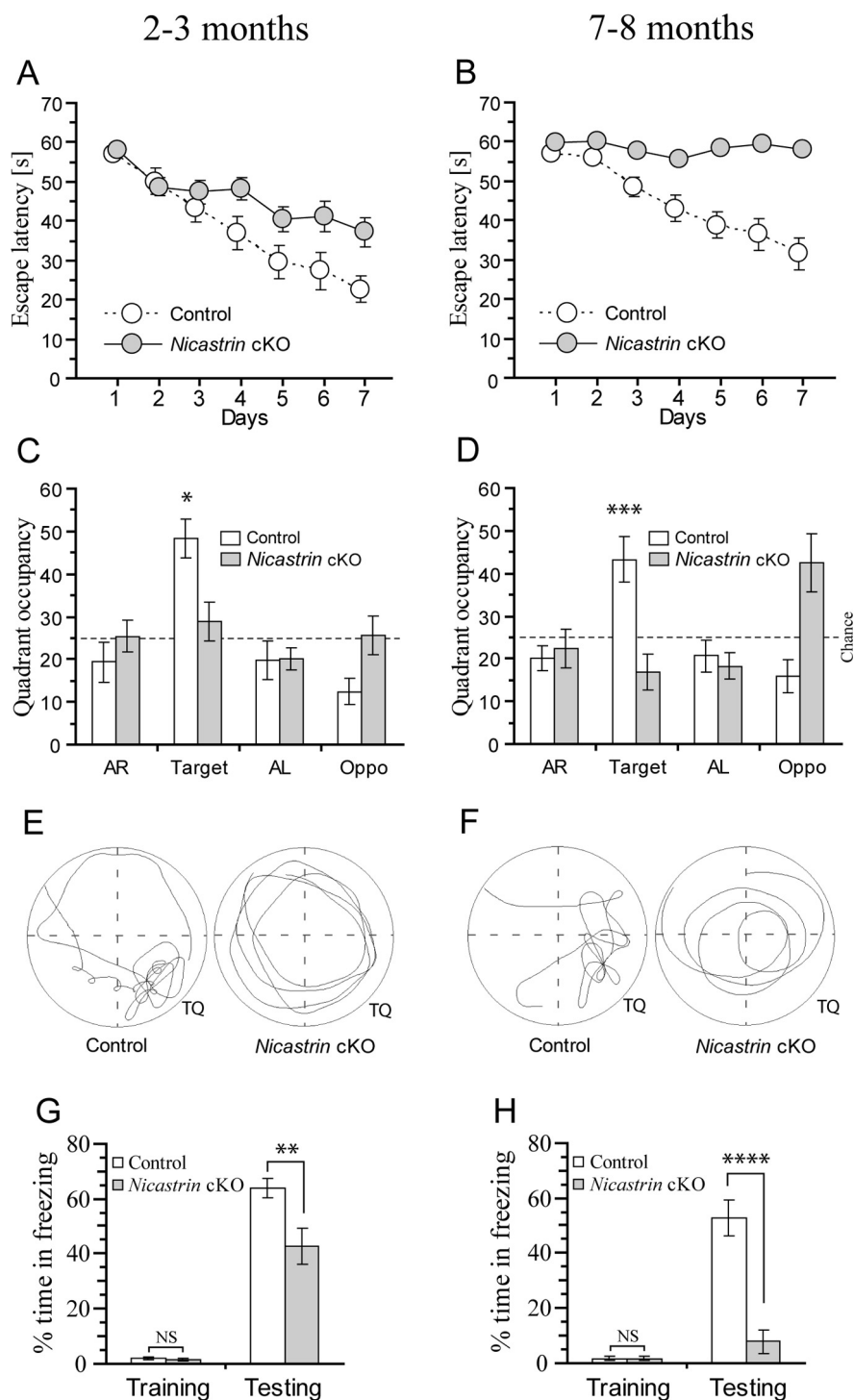
Figure 4. Progressive impairment of learning and memory in *nicastrin* cKO mice. *nicastrin* cKO and control mice at two different ages, 2–3 and 7–8 months, were examined in the Morris water maze to test spatial learning and memory, and in the contextual fear conditioning to test associative memory. ***A***, Escape latency in *nicastrin* cKO mice at 2–3 months. *nicastrin* cKO mice display longer escape latencies than age-matched littermate control animals across the 7 d training period ($n = 10$ for control; $n = 14$ for *nicastrin* cKO). Error bars indicate SEM. ***B***, Escape latency in *nicastrin* cKO mice at 7–8 months. Almost no improvement in escape latencies was observed in *nicastrin* cKO mice across the 7 d training period ($n = 15$ for control; $n = 11$ for *nicastrin* cKO). ***C***, Probe trial in *nicastrin* cKO mice at 2–3 months of age. Two- to three-month-old *nicastrin* cKO mice spend significantly less time searching for the platform in the target quadrant than the controls. The asterisk denotes statistical significance (*$p < 0.05$). AL, Adjacent left quadrant; T, target quadrant; AR, adjacent right quadrant; OP, opposite quadrant. Twenty-five percent is the chance performance during the probe trial. ***D***, Probe trial in *nicastrin* cKO mice at 7–8 months of age. The time spent in the target quadrant is dramatically decreased in 7- to 8-month-old *nicastrin* cKO mice compared with the controls ($F = 13.2$; df = 1, 24; $p < 0.001$). Of note, the time spent in the opposite quadrant in which they were initially released is significantly increased in the cKO group ($F = 12.9$; df = 1, 24; $p < 0.001$). The asterisks denote statistical significance (***$p < 0.001$). ***E***, ***F***, Representative swim paths for mice at 2–3 (***E***) and 7–8 (***F***) months of age during the posttraining probe trial. TQ, Target quadrant. ***G***, Percentage of

sensorimotor functions, we analyzed thigmotaxis during the hidden-platform training. We found no significant genotype effect on the time spent swimming 10 cm within the walls of the water maze (supplemental Fig. 1*A*, available at www.jneurosci.org as supplemental material), suggesting no abnormal anxiety levels in *nicastrin* cKO mice. We then performed a visible cued task to examine sensorimotor functions (supplemental Fig. 1*B*, available at www.jneurosci.org as supplemental material) and again found no significant genotype effect on the latency to find the visible platform. We examined open field activity and motor coordination using a cohort of naive mice at 2 months. We found no significant differences between the control and the cKO mice in horizontal activity, vertical activity, and total distance traveled in the open field (supplemental Fig. 2*A–C*, available at www.jneurosci.org as supplemental material). We found no significant genotype difference in latency to fall from the rotarod as well (supplemental Fig. 2*D*, available at www.jneurosci.org as supplemental material). These data suggest that impairment on spatial learning and memory is unlikely caused by abnormal sensorimotor functions.

Progressive impairment of contextual fear memory in *nicastrin* cKO mice
To investigate the effect of the loss of nicastrin on associative memory, we conducted a contextual fear conditioning task, in which robust hippocampus-dependent associative memory can be acquired in a single trial (Phillips and LeDoux, 1992). In this task, mice learn to associate a conditioned stimulus (test chamber) with an unconditioned stimulus (footshock). After pairing of the conditioned and unconditioned stimulus, the formation of an associative memory causes the presentation of the conditioned stimulus alone to elicit a fear response (e.g., freezing).

←

time spent in freezing in *nicastrin* cKO mice at 2–3 months of age in the contextual fear conditioning. *Nicastrin* cKO mice spend significantly less time freezing than age-matched littermate control animals 24 h after the footshock ($p < 0.01$; $n = 28$ for control; $n = 25$ for *nicastrin* cKO); however, they show indistinguishable levels of freezing to control mice during the training period. The asterisks denote statistical significance (**$p < 0.01$). NS denotes not significant. ***H***, Percentage of time in freezing in *nicastrin* cKO mice at 7–8 months of age in the contextual fear conditioning. *Nicastrin* cKO mice spend significantly less time freezing than the controls 24 h after the footshock ($p < 0.00001$; $n = 13$ for control; $n = 10$ for *Nicastrin* cKO), but they exhibit comparable levels of freezing to control mice during the training period. The asterisks denote statistical significance (****$p < 0.001$).

We examined 2–3 and 7– 8 months old *nicastrin* cKO and littermate control mice (Fig. 4*G*,*H*). An overall ANOVA was performed for all mice. First, the ANOVA revealed a highly significant within-subject effect ($F = 169.2$; df = 1, 72; $p < 0.00001$) on intervals (training vs 24 h postshock), suggestive of effective associative memory. Second, the ANOVA also revealed a highly significant main genotype effect ($F = 30.1$; df = 1, 72; $p < 0.00001$) and a highly significant interval by genotype interaction ($F = 32.3$; df = 1, 72; $p < 0.001$), suggesting impaired long-term associative fear memory in *nicastrin* cKO mice. Third, the ANOVA indicated a significant age effect ($F = 13.2$; df = 1, 72; $p < 0.001$), suggesting that the performance of older mice was worse than that of younger ones. We then performed data analysis for each age. At 2–3 months (Fig. 4*G*), *nicastrin* cKO mice displayed significantly less freezing 24 h after the footshock (control, 63.8 ± 3.6%; cKO, 42.7 ± 6.6%; $F = 8.3$; df = 1, 51; $p < 0.006$), but exhibited normal exploratory activity in the freezing chamber during the training period (control, 1.9 ± 0.5%; cKO, 1.4 ± 0.5%; $F < 1$), suggesting impaired associative memory. At 7– 8 months (Fig. 4*H*), *nicastrin* cKO mice again displayed significantly less freezing 24 h after the footshock (control, 52.7 ± 6.6%; cKO, 7.8 ± 4.1%; $F = 33.8$; df = 1, 21; $p < 0.000001$), whereas they showed normal exploratory activity during the training period (control, 1.6 ± 0.9%; cKO, 1.7 ± 0.7%; $F < 1$), indicating an even more severely impaired associative memory than at 2–3 months of age.

Interestingly, the overall ANOVA further revealed a significant interval by genotype by age interaction ($F = 5.4$; df = 1, 72; $p < 0.025$), suggesting that there is a progressive decline of fear associative memory in *nicastrin* cKO mice. We performed an ANOVA for the two control groups and found a highly significant within-subject effect on interval ($F = 266.0$; df = 1, 39; $p < 0.0001$) but no significant age effect ($F = 1.6$; df = 1, 39; $p > 0.2$). We also performed an ANOVA for the two cKO groups, and found a highly significant within-subject effect on interval ($F = 18.4$; df = 1, 33; $p < 0.0005$) and a highly significant age effect ($F = 11.9$; df = 1, 33; $p < 0.002$). Therefore, these data suggest a progressive decline of fear associative memory in *nicastrin* cKO mice.

**Age-dependent cortical neuronal loss in *nicastrin* cKO mice**
The age-related deterioration of memory in *nicastrin* cKO mice prompted us to examine whether loss of nicastrin in the adult cerebral cortex causes age-dependent anatomical alterations. We counted the total number of cortical neurons and measured the total cortical volume in *nicastrin* cKO mice at 6 and 9 months of age ($n = 4$ per genotype) using stereological method. Whereas the size of the cortex was normal in *nicastrin* cKO mice at 2 months (Fig. 3), we observed massive cortical atrophy at 6 and 9 months in *nicastrin* cKO mice (Fig. 5*A*). Our stereological quantification results showed that, compared with age-matched controls, the total cortical neuron number in the cKO group was
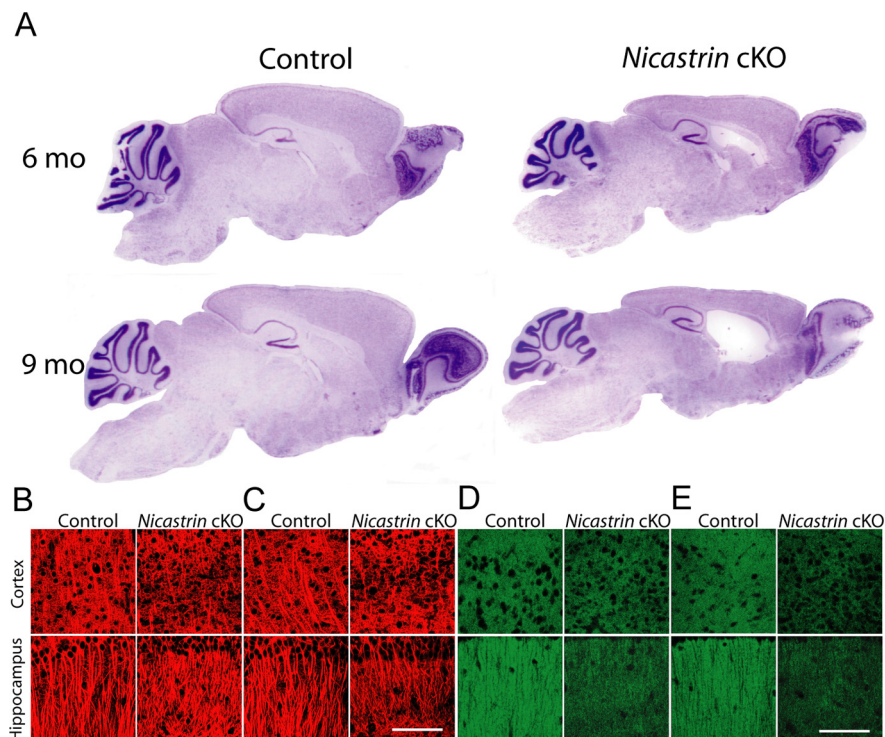
Figure 5. Progressive neurodegeneration in the cortex of *nicastrin* cKO mice. ***A***, Left, Nissl-stained sagittal brain sections of control mice at 6 and 9 months of age. Right, Nissl-stained brain sections of *nicastrin* cKO mice. There is progressive loss of white and gray matters in the neocortex and hippocampus and enlargement of lateral ventricles in 6- and 9-month-old *nicastrin* cKO mice. ***B***, Reduced MAP2 immunoreactivity in the neocortex and hippocampus of *nicastrin* cKO mice at 6 months of age. ***C***, Reduced MAP2 immunoreactivity in the neocortex and hippocampus of *nicastrin* cKO mice at 9 months of age. ***D***, Decreased synaptophysin immunoreactivity in the neocortex and hippocampus of *nicastrin* cKO mice at 6 months of age. ***E***, Decreased synaptophysin immunoreactivity in the neocortex and hippocampus of *nicastrin* cKO mice at 9 months of age. Scale bar, 100 μm.

significantly decreased at 6 (data not shown) and 9 months (data not shown). We performed an overall ANOVA on the total cortical neuron number for all three ages. The ANOVA revealed a highly significant main genotype effect ($F = 54.6$; df = 1, 16; $p < 0.0001$) and a highly significant genotype by age interaction effect ($F = 10.6$; df = 2, 16; $p < 0.005$), strongly suggesting a significant age-dependent neuronal loss in the cortex of *nicastrin* cKO mice. Our stereological results showed that the neocortical volume in cKO mice was significantly decreased at 6 (data not shown) and 9 months (data not shown). An overall ANOVA indicated a highly significant main genotype effect on cortical volume ($F = 206.4$; df = 1, 16; $p < 0.0001$) and a highly significant genotype by age interaction effect ($F = 45.8$; df = 2, 16; $p < 0.0001$), suggesting a striking age-dependent cortical atrophy in *nicastrin* cKO mice. Together, these results show that loss of nicastrin in the forebrain causes age-dependent cortical neuronal loss in mice.

We further performed immunohistological staining for MAP2 and synaptophysin using brain sections of *nicastrin* cKO mice at 6 and 9 months (Fig. 5*B–E*). We observed a significant reduction in MAP2 immunoreactivity in the neocortex and the hippocampus of *nicastrin* cKO mice at these two ages (Fig. 5 *B*, *C*). To quantify these changes, we performed Western analysis using cortical lysates from *nicastrin* cKO mice at 2 and 6 months of age using MAP2 antibodies (supplemental Fig. 3*A*, available at www.jneurosci.org as supplemental material). We found that MAP2 levels in *nicastrin* cKO mice kept unchanged at 2 months, but were reduced at 6 months. Our immunohistological data also revealed a progressive reduction on synaptophysin immunoreactivity in the neocortex and the hippocampus of *nicastrin* cKO
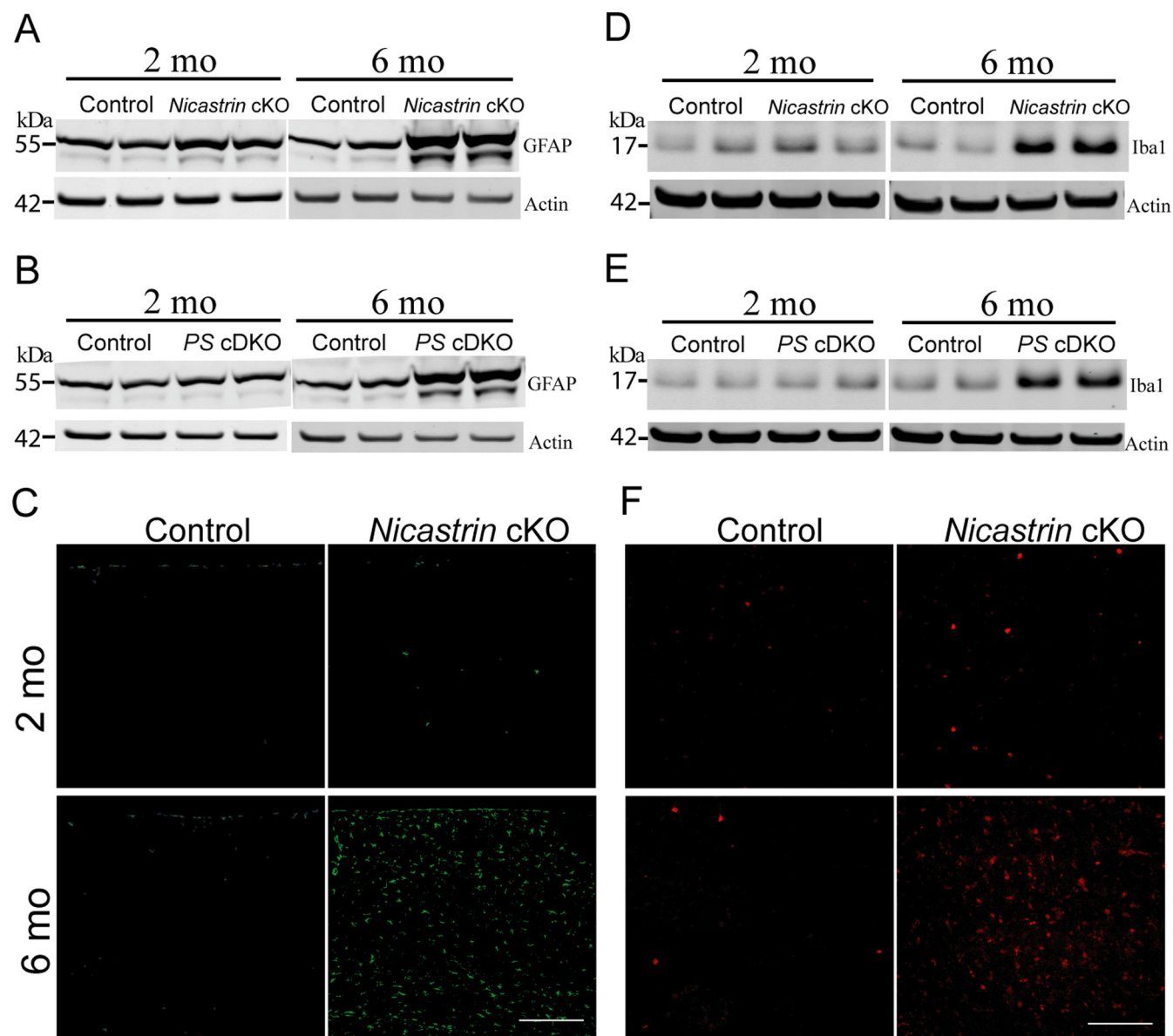
Figure 6. Progressive gliosis in *nicastrin* cKO and *PS* cDKO mice. **A**, Western analysis on protein levels of GFAP, a marker for astrocytes. There is a progressive increase of GFAP levels in cortical lysates of *nicastrin* cKO mice. At 2 months, GFAP levels are higher in *nicastrin* cKO mice ($p < 0.05$). However, at 6 months, there is an ∼3-fold increase in GFAP levels in the cortex of *nicastrin* cKO mice. **B**, Age-related increase of GFAP levels in *PS* cDKO mice. There is a small increase on GFAP levels between the control and *PS* cDKO mice at 2 months. At 6 months, there is a twofold increase in GFAP levels in *PS* cDKO mice. **C**, Immunostaining of GFAP in the neocortex of *nicastrin* cKO mice. There is a progressive astrocytosis in *nicastrin* cKO mice. In *nicastrin* cKO mice, there is a small increase in GFAP immunoreactivity at 2 months and a dramatic increase at 6 months. Scale bar, 200 μm. **D**, Western analysis on protein levels of Iba1, a marker for microglia. There is a progressive increase of Iba1 levels in cortical lysates of *nicastrin* cKO mice. At 2 months, Iba1 levels are higher in *nicastrin* cKO mice. At 6 months, there is a sixfold increase in Iba1 protein levels. **E**, Age-related increase of Iba1 levels in *PS* cDKO mice. There is a small increase in Iba1 levels in *PS* cDKO mice at 2 months and a threefold increase in Iba1 levels at 6 months. **F**, Immunostaining of Iba1 in the neocortex of *nicastrin* cKO mice. There is a progressive microgliosis in *nicastrin* cKO mice. Iba1 immunoreactivity is increased in the cKO cortex at 2 months and highly elevated at 6 months. Scale bar, 100 μm.

mice at 6 (Fig. 5*D*) and 9 (Fig. 5*E*) months. Our Western analysis in synaptophysin using cortical lysates at 2 and 6 months confirmed an age-related reduction (supplemental Fig. 3*B*, available at www.jneurosci.org as supplemental material). These results indicate age-dependent loss of dendrites and synapses in aging *nicastrin* cKO mice.

Progressive gliosis in *nicastrin* cKO mice
Since neurodegeneration is often accompanied by inflammatory responses, we assessed the levels of inflammatory markers in *nicastrin* cKO mice. To examine whether there is ongoing, progressive astrogliosis in the *nicastrin* cKO cortex, we performed Western analysis on GFAP, a marker for reactive astrocytes, using

cortical lysates at 2 and 6 months. We found that there was a small but significant increase in GFAP levels in *nicastrin* cKO mice at 2 months (Fig. 6*A*) (133 ± 8.0% of *nicastrin* cKO vs 100 ± 9.1% of control; $p < 0.025$) and a robust increase at 6 months (Fig. 6*A*) (399 ± 20.0% of *nicastrin* cKO vs 100 ± 23.3% of control; $p < 0.005$). In parallel, we conducted Western analysis on GFAP using cortical lysates of *PS* cDKO mice at 2 and 6 months, and also observed an age-dependent increase in GFAP levels (Fig. 6*B*). We then conducted GFAP immunostaining using brain sections of *nicastrin* cKO mice at 2, 6, and 9 months. GFAP immunoreactivity showed a small increase in the neocortex (Fig. 6*C*) but no change in the hippocampus (supplemental Fig. 4*A*, available at www.jneurosci.org as supplemental material) at 2 months; how-
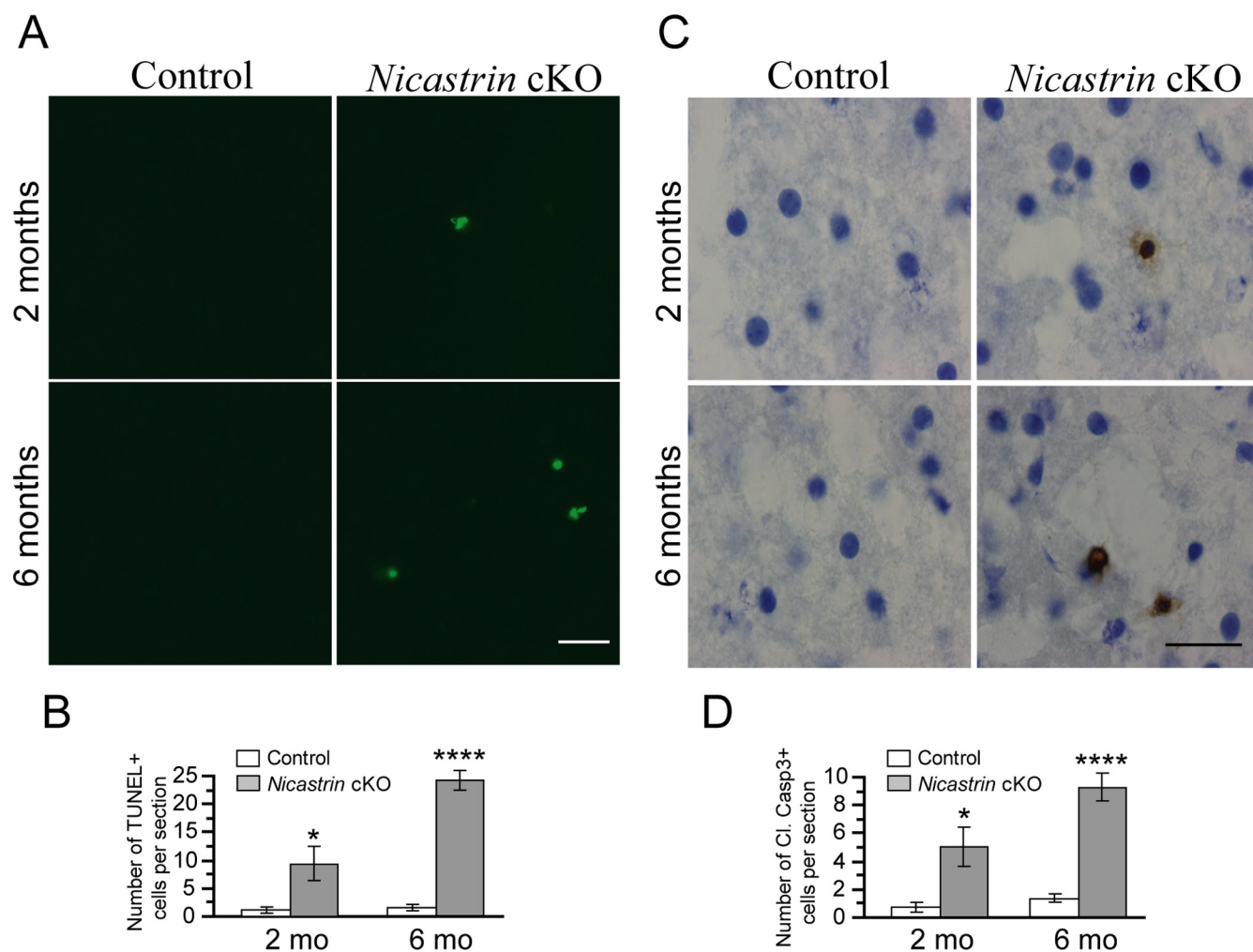
Figure 7. Increased apoptotic cells in *nicastrin* cKO mice. ***A***, TUNEL staining in the neocortex of *nicastrin* cKO mice. TUNEL cells are shown in green. At 2 months, TUNEL cells can be seen in the cortex of *nicastrin* cKO mice. However, many more TUNEL cells can be found in *nicastrin* cKO mice at 6 months. Control mice do not show TUNEL cells. Scale bar, 25 μm. ***B***, Quantitative data on the average number of TUNEL cells per section. At 2 months, *nicastrin* cKO mice show more TUNEL cells in the cortex than control mice (control, $n = 4$; cKO, $n = 5$). At 6 months, there is a highly significant increase on the average number of TUNEL cells in *nicastrin* cKO mice (control, $n = 4$; cKO, $n = 5$). Error bars indicate SEM. The asterisks denote statistical significance (*$p < 0.05$; ****$p < 0.001$). ***C***, Active caspase-3 immunostaining in the neocortex of *nicastrin* cKO mice. The sections were counterstained with hematoxylin. Active caspase-3-positive (+) cells are shown in brown and nonactive caspase-3-positive cells are shown in blue. At 2 months, active caspase-3-positive staining can be seen in *nicastrin* cKO mice. At 6 months, *nicastrin* cKO mice show many more cells with positive staining for active caspase-3 in the cortex. Scale bar, 25 μm. ***D***, Quantification of average numbers of active caspase-3 cells per section. At 2 months, the average number of active caspase-3 is higher in *nicastrin* cKO than control mice (control, $n = 4$; cKO, $n = 5$). At 6 months, there is a large increase in the average number of active caspase-3 cells in *nicastrin* cKO mice (control, $n = 4$; cKO, $n = 5$).

ever, GFAP immunoreactivity became progressively elevated in the neocortex (Fig. 6C) and in the hippocampus (supplemental Fig. 4A, available at www.jneurosci.org as supplemental material) at 6 and 9 months of age. These data demonstrate a progressive astrocytosis in *nicastrin* cKO mice.

In a second set of experiments, we investigated microgliosis in the mutant mice. We conducted Western analysis on ionized calcium-binding adapter molecule 1 (Iba1), which is specifically expressed in microglia in the brain (Imai et al., 1996), using cortical lysates at 2 and 6 months. We observed a significant increase in Iba1 levels at 2 months (Fig. 6D) (164 $\pm$ 23.7% of *nicastrin* cKO vs 100 $\pm$ 16.1% of control; $p < 0.05$) and a very large increase at 6 months (Fig. 6D) (669 $\pm$ 108.6% of *nicastrin* cKO vs 100 $\pm$ 9.2% of control; $p < 0.05$). We also performed Western analysis on Iba1 using cortical lysates of *PS* cDKO mice at 2 and 6 months and found a progressive increase as well (Fig. 6E). We then conducted Iba1 immunohistochemistry. There was a small increase on Iba1 immunoreactivity in the neocortex (Fig. 6F) and

the hippocampus (supplemental Fig. 4B, available at www.jneurosci.org as supplemental material) at 2 months. In contrast, 6-month-old *nicastrin* cKO mice showed robust increased Iba1 immunoreactivity in the neocortex (Fig. 6F) and the hippocampus (supplemental Fig. 4B, available at www.jneurosci.org as supplemental material), consistent with progressive microgliosis.

Increased apoptotic cells in *nicastrin* cKO mice
To determine whether neurons in *nicastrin* cKO mice die via apoptosis, we performed the TUNEL assay using mice at 2 and 6 months of age. We observed a significant increase in the number of TUNEL-positive (TUNEL+) cells in the neocortex of *nicastrin* cKO mice at 2 months, compared with the control (Fig. 7A,B) (number of TUNEL+ cells per section: *nicastrin* cKO, 9.3 $\pm$ 3; control, 1.1 $\pm$ 0.4; $p < 0.05$; $n = 4$–5 per group), although the apoptotic cells represent a very small percentage of all cortical neurons (~0.05%). Similarly, many more TUNEL+ cells were found in the cortex of *nicastrin* cKO mice at 6 months (Fig. 7)

(*nicastrin* cKO, 24.1 ± 1.8, vs control, 1.5 ± 0.4; $p < 0.00001$; $n = 4$–5 per group). We also found a significant change in the number of cells that are positive for active caspase-3 immunostaining in the neocortex of *nicastrin* cKO mice at 2 months (Fig. 7*C,D*) (number of active caspase-3 positive cells per section: cKO, 5.0 ± 1.4; control, 0.7 ± 0.3; $p < 0.05$; $n = 4$–5 per group). Furthermore, at 6 months of age, we observed many more cells that are positive for active caspase-3 in the cortex of *nicastrin* cKO mice (cKO, 9.1 ± 1.0, vs control, 1.3 ± 0.3; $p < 0.0005$; $n = 4$–5 per group). These results demonstrate an ongoing and progressive apoptosis in *nicastrin* cKO mice.

Discussion

Presenilin is a key subunit of the γ-secretase complex, which is responsible for the cleavage of APP, Notch, and other substrates, and performs essential functions during development and intercellular signaling (Selkoe and Kopan, 2003). Recent studies suggested that in mature, fully developed animals, presenilins are additionally required for neuronal survival and memory formation (Yu et al., 2001; Feng et al., 2004; Saura et al., 2004), although the mechanism remained unclear. In addition to functioning as a γ-secretase subunit, presenilin possesses γ-secretase independent activities, such as the regulation of Ca^{2+} release from the endoplasmic reticulum (De Strooper et al., 1998, 1999; Kang et al., 1999, 2002; Ni et al., 2001; Kim et al., 2002, 2005; LaFerla, 2002; Lammich et al., 2002; Lee et al., 2002; Marambaud et al., 2002; Murakami et al., 2003; Tu et al., 2006). Thus, the question arose whether presenilins support neuronal survival and memory formation by a γ-secretase-dependent or γ-secretase-independent mechanism. Indeed, studies testing the effects of pathogenic presenilin mutants on Ca^{2+} release from the endoplasmic reticulum suggested that the pathogenic mutations represent a partial loss of this particular function, in a γ-secretase-independent manner, and further suggested that this γ-secretase-independent activity of presenilin may be responsible for neurodegeneration in Alzheimer's disease (Nelson et al., 2007; Bezprozvanny and Mattson, 2008).

To address this central question, we focused on nicastrin, which like presenilins serves as an essential component of the γ-secretase complex (Yu et al., 2000; De Strooper, 2003). We investigated the effects of the deletion of *nicastrin* on neuronal survival and memory formation. Similar to *PS* germline deletion mice (Shen et al., 1997; Donoviel et al., 1999), constitutive *nicastrin* KO mice die during embryonic development (Li et al., 2003a,b), making it impossible to study the physiological function of nicastrin in the adult brain in such KO mice. To overcome this problem, we chose the same strategy as we previously used for presenilins (Yu et al., 2001; Saura et al., 2004), and generated conditional *nicastrin* KO mice (Fig. 1). Unlike conventional *nicastrin* KO mice (Li et al., 2003a,b), *nicastrin* cKO mice are viable, appear to be indistinguishable from their littermate controls during their first months of life, and exhibit no major developmental changes (data not shown) (Fig. 3). We characterized the *nicastrin* cKO mice as a function of age and compared them with *PS* cDKO mice. Our results demonstrate that *nicastrin* cKO mice exhibit the same striking phenotype as *PS* cDKO mice, suggesting that γ-secretase activity is required for the function and survival of mature neurons. Three major observations were made in the current study.

First, *nicastrin* cKO mice display a series of biochemical changes consistent with its function as a γ-secretase subunit. The levels of APP-CTFs, major presynaptic γ-secretase substrates, are increased massively, whereas the levels of APP and soluble αAPPs (produced by α-secretase cleavage) are unchanged (Fig. 2*C*), similar to what was previously observed in *PS1* cKO and *PS* cDKO mice (Yu et al., 2001; Saura et al., 2004, 2005). Moreover, the abundance of two other γ-secretase subunits, PS1, which is physiologically cleaved into N- and C-terminal fragments, and Pen-2, are decreased on deletion of *nicastrin* (Fig. 2*A*). Interestingly, Pen-2 is also decreased in *PS* cDKO mice (Fig. 2*B*), consistent with recent *in vitro* findings (Edbauer et al., 2002; Hu et al., 2002), indicating that most of the γ-secretase subunits depend on each other for stability. Although four γ-secretase subunits can regulate each other, Aph-1 is least sensitive to changes in expression of the others (De Strooper, 2003). Our findings on unchanged protein levels of Aph-1a in both *nicastrin* cKO and *PS* cDKO mice are consistent with a previous study (Gu et al., 2003).

Second, *nicastrin* cKO mice exhibit impairment of learning and memory at 2–3 months of age (Fig. 4), when there is no significant loss of synapses or neurons (Fig. 3). The memory impairment was observed using both Morris water maze and fear conditioning paradigms and is as severe as those observed in *PS* cDKO mice (Saura et al., 2004). The severity of learning and memory impairment increases with age in *nicastrin* cKO mice, such that, at 7–8 months, the mutant mice are completely refractory to learning (Fig. 4).

Last, *nicastrin* cKO mice develop an age-related, progressive neurodegeneration (Figs. 5, 7), which is as severe as that observed in *PS* cDKO mice (Saura et al., 2004). The neurodegeneration results in a loss of ∼37% of cortical neurons and a 44% shrinkage of the cortical volume at 9 months (Fig. 5). Compared with control mice, a significant increase in apoptotic neurons is already apparent at 2 months of age in *nicastrin* cKO mice, and by 6 months of age the increase in apoptotic neurons is dramatic (Fig. 7). However, the small number of apoptotic neurons found in the cerebral cortex of *nicastrin* cKO mice at 2 months is insufficient to cause a significant reduction in the total cortical neuron number and the cortical volume. In response to the ongoing cell death, astrocytes and microglia initiate inflammatory responses, which are detectable at 2 months of age and also increase dramatically during aging (Fig. 6). A similar severity of gliosis was detected in *PS* cDKO mice (Beglopoulos et al., 2004; Saura et al., 2004). Moreover, following up on previous evidence suggesting that accumulation of hyperphosphorylated tau plays an important role in neurodegeneration in AD (Trojanowski and Lee, 2002), we found that hyperphosphorylated tau levels are also increased at 6 months of age (supplemental Fig. 5, available at www.jneurosci.org as supplemental material).

Thus, our results demonstrate that deletion of either of the two γ-secretase subunits in mature, fully developed neurons leads to very similar phenotypes, composed of a general destabilization of γ-secretase complex, a progressive learning and memory impairment, and a severe age-dependent and progressive neurodegeneration. Among others, these data strongly suggest that presenilin and nicastrin maintain neuronal survival through a γ-secretase-dependent mechanism, rather than a γ-secretase-independent activity, such as a presenilin-specific role in regulating Ca^{2+} release from the endoplasmic reticulum. Furthermore, our data—including the increase in tau phosphorylation, and the widespread apoptosis—are consistent with the notion that the neurodegeneration induced by inactivation of γ-secretase subunits resembles the neurodegeneration observed in AD. This notion reinforces the need to reconsider the use of γ-secretase inhibitors as potential treatments of AD and indicates that much additional work is required to evaluate their potential utility.

Although conclusive with regard to a γ-secretase-dependent

mechanism of neurodegeneration, our data do not reveal why γ-secretase inactivation produces neurodegeneration. At least two principal possibilities exist. First, after γ-secretase inactivation, accumulation of a particular uncleaved γ-secretase substrate, such as the APP-CTFs, may be neurotoxic, although this was ruled out at least for APP-CTFs (Rutten et al., 2003). Second, inactivation of γ-secretase may impair an essential cellular signaling pathway, thereby depriving the neurons of a required signal involved in synapse function and survival. Candidates for such a function include APP (Cao and Südhof, 2001), Notch (De Strooper et al., 1999), and cadherins (Marambaud et al., 2002). However, the lack of conditional knock-out mouse for each of these genes makes it difficult to determine which of these or additional γ-secretase substrates may be responsible for PS-dependent memory and neuronal survival. Uncovering the pathway(s) to neurodegeneration in *nicastrin* cKO and *PS* cDKO mice will be important for developing potential new avenues to treating neurodegeneration and can now be approached with the availability of these mice.

References

Beglopoulos V, Sun X, Saura CA, Lemere CA, Kim RD, Shen J (2004) Reduced beta-amyloid production and increased inflammatory responses in presenilin conditional knock-out mice. J Biol Chem 279:46907–46914.

Bezprozvanny I, Mattson MP (2008) Neuronal calcium mishandling and the pathogenesis of Alzheimer's disease. Trends Neurosci 31:454–463.

Brown MS, Ye J, Rawson RB, Goldstein JL (2000) Regulated intramembrane proteolysis: a control mechanism conserved from bacteria to humans. Cell 100:391–398.

Cao X, Südhof TC (2001) A transcriptively active complex of APP with Fe65 and histone acetyltransferase Tip60. Science 293:115–120.

Chen F, Yu G, Arawaka S, Nishimura M, Kawarai T, Yu H, Tandon A, Supala A, Song YQ, Rogaeva E, Milman P, Sato C, Yu C, Janus C, Lee J, Song L, Zhang L, Fraser PE, St. George-Hyslop PH (2001) Nicastrin binds to membrane-tethered Notch. Nat Cell Biol 3:751–754.

Chung HM, Struhl G (2001) Nicastrin is required for Presenilin-mediated transmembrane cleavage in *Drosophila*. Nat Cell Biol 3:1129–1132.

De Strooper B (2003) Aph-1, Pen-2, and Nicastrin with Presenilin generate an active gamma-Secretase complex. Neuron 38:9–12.

De Strooper B, Saftig P, Craessaerts K, Vanderstichele H, Guhde G, Annaert W, Von Figura K, Van Leuven F (1998) Deficiency of presenilin-1 inhibits the normal cleavage of amyloid precursor protein. Nature 391:387–390.

De Strooper B, Annaert W, Cupers P, Saftig P, Craessaerts K, Mumm JS, Schroeter EH, Schrijvers V, Wolfe MS, Ray WJ, Goate A, Kopan R (1999) A presenilin-1-dependent gamma-secretase-like protease mediates release of Notch intracellular domain. Nature 398:518–522.

Donoviel DB, Hadjantonakis AK, Ikeda M, Zheng H, Hyslop PS, Bernstein A (1999) Mice lacking both presenilin genes exhibit early embryonic patterning defects. Genes Dev 13:2801–2810.

Dymecki SM (1996) Flp recombinase promotes site-specific DNA recombination in embryonic stem cells and transgenic mice. Proc Natl Acad Sci U S A 93:6191–6196.

Edbauer D, Winkler E, Haass C, Steiner H (2002) Presenilin and nicastrin regulate each other and determine amyloid beta-peptide production via complex formation. Proc Natl Acad Sci U S A 99:8666–8671.

Feng R, Wang H, Wang J, Shrom D, Zeng X, Tsien JZ (2004) Forebrain degeneration and ventricle enlargement caused by double knockout of Alzheimer's presenilin-1 and presenilin-2. Proc Natl Acad Sci U S A 101:8162–8167.

Fortini ME (2002) Gamma-secretase-mediated proteolysis in cell-surface-receptor signalling. Nat Rev Mol Cell Biol 3:673–684.

Gu Y, Chen F, Sanjo N, Kawarai T, Hasegawa H, Duthie M, Li W, Ruan X, Luthra A, Mount HT, Tandon A, Fraser PE, St. George-Hyslop P (2003) APH-1 interacts with mature and immature forms of presenilins and nicastrin and may play a role in maturation of presenilin-nicastrin complexes. J Biol Chem 278:7374–7380.

Hardy J, Selkoe DJ (2002) The amyloid hypothesis of Alzheimer's disease: progress and problems on the road to therapeutics. Science 297:353–356.

Ho A, Morishita W, Atasoy D, Liu X, Tabuchi K, Hammer RE, Malenka RC, Südhof TC (2006) Genetic analysis of Mint/X11 proteins: essential presynaptic functions of a neuronal adaptor protein family. J Neurosci 26:13089–13101.

Hu Y, Ye Y, Fortini ME (2002) Nicastrin is required for gamma-secretase cleavage of the *Drosophila* Notch receptor. Dev Cell 2:69–78.

Imai Y, Ibata I, Ito D, Ohsawa K, Kohsaka S (1996) A novel gene iba1 in the major histocompatibility complex class III region encoding an EF hand protein expressed in a monocytic lineage. Biochem Biophys Res Commun 224:855–862.

Kang DE, Soriano S, Frosch MP, Collins T, Naruse S, Sisodia SS, Leibowitz G, Levine F, Koo EH (1999) Presenilin 1 facilitates the constitutive turnover of beta-catenin: differential activity of Alzheimer's disease-linked PS1 mutants in the beta-catenin-signaling pathway. J Neurosci 19:4229–4237.

Kang DE, Soriano S, Xia X, Eberhart CG, De Strooper B, Zheng H, Koo EH (2002) Presenilin couples the paired phosphorylation of beta-catenin independent of axin: implications for beta-catenin activation in tumorigenesis. Cell 110:751–762.

Kim DY, Ingano LA, Kovacs DM (2002) Nectin-1alpha, an immunoglobulin-like receptor involved in the formation of synapses, is a substrate for presenilin/gamma-secretase-like cleavage. J Biol Chem 277:49976–49981.

Kim DY, Ingano LA, Carey BW, Pettingell WH, Kovacs DM (2005) Presenilin/gamma-secretase-mediated cleavage of the voltage-gated sodium channel beta2-subunit regulates cell adhesion and migration. J Biol Chem 280:23251–23261.

LaFerla FM (2002) Calcium dyshomeostasis and intracellular signalling in Alzheimer's disease. Nat Rev Neurosci 3:862–872.

Lammich S, Okochi M, Takeda M, Kaether C, Capell A, Zimmer AK, Edbauer D, Walter J, Steiner H, Haass C (2002) Presenilin-dependent intramembrane proteolysis of CD44 leads to the liberation of its intracellular domain and the secretion of an Abeta-like peptide. J Biol Chem 277:44754–44759.

Lee SF, Shah S, Li H, Yu C, Han W, Yu G (2002) Mammalian APH-1 interacts with presenilin and nicastrin and is required for intramembrane proteolysis of amyloid-beta precursor protein and Notch. J Biol Chem 277:45013–45019.

Li J, Fici GJ, Mao CA, Myers RL, Shuang R, Donoho GP, Pauley AM, Himes CS, Qin W, Kola I, Merchant KM, Nye JS (2003a) Positive and negative regulation of the gamma-secretase activity by nicastrin in a murine model. J Biol Chem 278:33445–33449.

Li T, Ma G, Cai H, Price DL, Wong PC (2003b) Nicastrin is required for assembly of presenilin/gamma-secretase complexes to mediate Notch signaling and for processing and trafficking of beta-amyloid precursor protein in mammals. J Neurosci 23:3272–3277.

López-Schier H, St. Johnston D (2002) *Drosophila* nicastrin is essential for the intramembranous cleavage of notch. Dev Cell 2:79–89.

Marambaud P, Shioi J, Serban G, Georgakopoulos A, Sarner S, Nagy V, Baki L, Wen P, Efthimiopoulos S, Shao Z, Wisniewski T, Robakis NK (2002) A presenilin-1/gamma-secretase cleavage releases the E-cadherin intracellular domain and regulates disassembly of adherens junctions. EMBO J 21:1948–1956.

Morris RG, Garrud P, Rawlins JN, O'Keefe J (1982) Place navigation impaired in rats with hippocampal lesions. Nature 297:681–683.

Murakami D, Okamoto I, Nagano O, Kawano Y, Tomita T, Iwatsubo T, De Strooper B, Yumoto E, Saya H (2003) Presenilin-dependent gamma-secretase activity mediates the intramembranous cleavage of CD44. Oncogene 22:1511–1516.

Nelson O, Tu H, Lei T, Bentahir M, de Strooper B, Bezprozvanny I (2007) Familial Alzheimer disease-linked mutations specifically disrupt Ca^{2+} leak function of presenilin 1. J Clin Invest 117:1230–1239.

Nguyen V, Hawkins C, Bergeron C, Supala A, Huang J, Westaway D, St. George-Hyslop P, Rozmahel R (2006) Loss of nicastrin elicits an apoptotic phenotype in mouse embryos. Brain Res 1086:76–84.

Ni CY, Murphy MP, Golde TE, Carpenter G (2001) gamma-Secretase cleavage and nuclear localization of ErbB-4 receptor tyrosine kinase. Science 294:2179–2181.

Phillips RG, LeDoux JE (1992) Differential contribution of amygdala and hippocampus to cued and contextual fear conditioning. Behav Neurosci 106:274–285.

Price DL, Tanzi RE, Borchelt DR, Sisodia SS (1998) Alzheimer's disease: genetic studies and transgenic models. Annu Rev Genetics 32:461–493.

Rutten BP, Wirths O, Van de Berg WD, Lichtenthaler SF, Vehoff J, Steinbusch HW, Korr H, Beyreuther K, Multhaup G, Bayer TA, Schmitz C (2003) No alterations of hippocampal neuronal number and synaptic bouton number in a transgenic mouse model expressing the beta-cleaved C-terminal APP fragment. Neurobiol Dis 12:110–120.

Saura CA, Choi SY, Beglopoulos V, Malkani S, Zhang D, Shankaranarayana Rao BS, Chattarji S, Kelleher RJ 3rd, Kandel ER, Duff K, Kirkwood A, Shen J (2004) Loss of presenilin function causes impairments of memory and synaptic plasticity followed by age-dependent neurodegeneration. Neuron 42:23–36.

Saura CA, Chen G, Malkani S, Choi SY, Takahashi RH, Zhang D, Gouras GK, Kirkwood A, Morris RG, Shen J (2005) Conditional inactivation of presenilin 1 prevents amyloid accumulation and temporarily rescues contextual and spatial working memory impairments in amyloid precursor protein transgenic mice. J Neurosci 25:6755–6764.

Selkoe D, Kopan R (2003) Notch and Presenilin: regulated intramembrane proteolysis links development and degeneration. Annu Rev Neurosci 26:565–597.

Shah S, Lee SF, Tabuchi K, Hao YH, Yu C, LaPlant Q, Ball H, Dann CE 3rd, Südhof T, Yu G (2005) Nicastrin functions as a gamma-secretase-substrate receptor. Cell 122:435–447.

Shen J, Bronson RT, Chen DF, Xia W, Selkoe DJ, Tonegawa S (1997) Skeletal and CNS defects in Presenilin-1-deficient mice. Cell 89:629–639.

Steiner H, Winkler E, Edbauer D, Prokop S, Basset G, Yamasaki A, Kostka M, Haass C (2002) PEN-2 is an integral component of the gamma-secretase complex required for coordinated expression of presenilin and nicastrin. J Biol Chem 277:39062–39065.

Trojanowski JQ, Lee VM (2002) The role of tau in Alzheimer's disease. Med Clin North Am 86:615–627.

Tu H, Nelson O, Bezprozvanny A, Wang Z, Lee SF, Hao YH, Serneels L, De Strooper B, Yu G, Bezprozvanny I (2006) Presenilins form ER Ca^{2+} leak channels, a function disrupted by familial Alzheimer's disease-linked mutations. Cell 126:981–993.

West MJ, Gundersen HJ (1990) Unbiased stereological estimation of the number of neurons in the human hippocampus. J Comp Neurol 296:1–22.

Yu G, Nishimura M, Arawaka S, Levitan D, Zhang L, Tandon A, Song YQ, Rogaeva E, Chen F, Kawarai T, Supala A, Levesque L, Yu H, Yang DS, Holmes E, Milman P, Liang Y, Zhang DM, Xu DH, Sato C, et al. (2000) Nicastrin modulates presenilin-mediated notch/glp-1 signal transduction and betaAPP processing. Nature 407:48–54.

Yu H, Saura CA, Choi SY, Sun LD, Yang X, Handler M, Kawarabayashi T, Younkin L, Fedeles B, Wilson MA, Younkin S, Kandel ER, Kirkwood A, Shen J (2001) APP processing and synaptic plasticity in presenilin-1 conditional knockout mice. Neuron 31:713–726.